Available online at www.sciencedirect.com
ScienceDirect
Journal of the European Ceramic Society 27 (2007) 3117–3125
www.elsevier.com/locate/jeurceramsoc

Drying stress of yttria-stabilized-zirconia slurry on a metal substrate

Weihua Lan, Ping Xiao *

School of Materials, University of Manchester, Manchester M1 7HS, UK

Received 8 November 2006; accepted 7 January 2007
Available online 12 March 2007

Abstract

Aqueous yttria-stabilized-zirconia (YSZ) nano-particle slurries (termed as nano-slurries later) were cast on metal substrates to form wet coatings. Stress development was measured using a substrate reflection method, coupled with drying kinetics measurements and coating structure examination. Lateral drying occurred and was controlled by the viscosity of the slurry. Tensile stress was generated due to constrained shrinkage of the wet coating when the slurry became saturated with water, starting from the coating edge when the solid concentration reached a certain level. As the saturated region extended to the centre, the stress increased to the maximum, then dropped quickly to zero due to cracking and delamination. Addition of micro-sized particles to the nano-slurry resulted in reduction of the peak stress while no apparent cracks were formed during drying. In addition, non-zero residual stress remained after drying, suggesting good bonding between the coating and the substrate.

Keywords: Drying; Slurry; Coating; Stress; Cracking

1. Introduction

Colloidal processes, including tape casting,[1] dip coating,[2] slurry coating[3] and electrophoretic deposition (EPD),[4] have been used to produce thin films and coatings. A powder suspension or slurry is applied to a substrate, and evaporation of the solvent concentrates the particles into a powder network. Concave menisci form at the air-liquid interface in the powder network and compress the powder network to contract further.[5] Because the contraction is resisted by the substrate and mostly occurs in the thickness direction, in-plane tensile stress arises in the coating, and leads to crack formation and, sometimes, coating delamination.

Stress development in ceramic coatings prepared by colloidal methods has been extensively studied. Chiu et al.[6,7] and Guo et al.[8] studied the drying of coatings composed of ceramic particles and solvent without organic binders. They measured in situ stress evolution using the optical interference method and attributed the tensile stress to the capillary force in the wet coating, which reached the maximum when the air–liquid interface began to recede into the coating, then decayed to zero or a lower residual stress when liquid drained from the pores in the coating. When the stress exceeded the cohesive strength of the coating, cracks formed and propagated. These failures could be avoided by reducing the coating thickness or the stress. Critical coating thickness above which failures occurred[2,6–8] could be decided by carrying out statistical experiments. The stress could be reduced by decreasing liquid surface tension or increasing particle/agglomerate size in the coating.[7–10]

The drying of a wet coating on a plane substrate has been observed to proceed from the edge, which is termed as lateral drying.[6–8,11,12] During the drying process, a water-saturated region, where water is just enough to completely fill the pore space between densely packed particles, forms first at the coating edge, while a water-supersaturated region, where water content is over that required to completely fill the pore space between densely packed particles and particles are suspended to migrate freely, remains at the center.[13] Lateral flow of free particles and liquid is driven by the capillary force from the centre to the edge. The distance over which the lateral flow occurs is defined as the capillary length. When the capillary length is equal to or longer than the specimen half-length, the coating is uniformly saturated with water, which is the case for Chiu et al.[6,7] and Guo et al.[8] They found that the maximum stress was reached after

* Corresponding author. Tel.: +44 161 306 5941; fax: +44 161 306 3586.
E-mail address: ping.xiao@manchester.ac.uk (P. Xiao).

0955-2219/$ – see front matter © 2007 Elsevier Ltd. All rights reserved.
doi:10.1016/j.jeurceramsoc.2007.01.005

the central fluid region disappeared and the whole coating was saturated with water. However, there was no study on how the lateral flow affected the stress evolution. Recently, Tirumkudulu and Russel[14] theoretically proved that the tensile stress mainly developed in the water-saturated region. The uneven water distribution due to the lateral flow certainly would affect stress evolution. When the capillary length is shorter than the specimen half-length, liquid would be drained from the edge where air–liquid interface recedes into pores and cracks might form. The stress evolution would be complicated by the coexistence of the cracking region, the water-saturated region and the water-supersaturated region. However, to our knowledge such study has not been carried out.

In this work, aqueous YSZ nano-slurries were cast on metal substrates to form wet coatings and dried under the constrained stress from the substrate. Lateral drying was observed by in situ monitoring of the coating surface. Non-uniform water saturation across the coating surface was found with three domains, i.e. a cracked region, a water-saturated region and a water-supersaturated region. Tensile stress was generated due to the constrained volume shrinkage, and rose when the saturated region appeared at the coating edge. The relation between lateral drying and stress development was discussed as a function of the initial water content and the agglomeration degree of the nano-slurries. Meanwhile, the drying kinetics was characterized by measuring the in situ weight loss of the wet coating. Due to high tensile stress, coatings prepared from nano-slurries cracked into fragments and delaminated from substrates. Micro-sized particles were added to the nano-slurry to decrease the tensile stress, leading to formation of coatings without destructive cracks.

2. Experimental procedure

2.1. Materials

Aqueous YSZ nano-slurry (MEL Chemicals, Manchester, UK) was used as a starting material, which has a composition of 8 wt% Y_2O_3–ZrO_2, a solid content of 25 wt%, a pH value of 1.5, a ξ-potential of 35.5 mV, and a specific surface area of 7.8×10^4 m^2/kg. The TEM micrograph (Fig. 1a) shows that the nano-particles have spherical morphology with primary particle size around 15 nm which is close to the calculated particle size, 12.7 nm, from the specific surface area.

Dilute sodium hydroxide (NaOH) solution was added to the as-received nano-slurry with continuous magnetic stirring to induce different agglomeration degrees.[12] After 24 h stirring, the nano-slurries were concentrated to higher solid content by drying at room temperature. Nano-slurries with initial water content in the range of 50–70 wt% and pH value in the range of 1.5–7.5 were used for drying experiments.

'Binary particle' slurries were prepared by adding micro-particles to the as-received nano-slurry with continuous magnetic stirring. Two micro-particles (MEL Chemicals, Manchester, UK and Daiichi Kigenso Kagaku Kogyo, Japan) were used, of which the SEM micrographs are shown in Fig. 1b and c. The average particle size was calculated as 0.17 and 5 μm, respectively, according to their specific surface areas, 5.8×10^3 and 2×10^2 m^2/kg. The volume ratio between nano-particles and micro-particles was controlled as 1:5. The water content of the 'binary particle' slurries was adjusted to around 26 wt% by drying at room temperature.

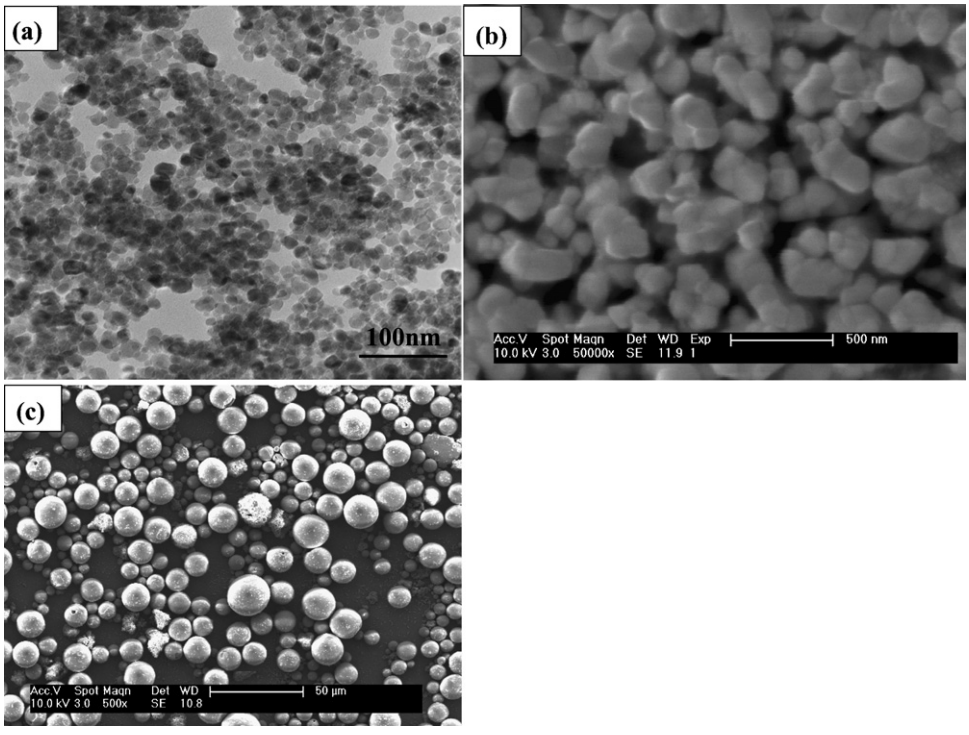

Fig. 1. (a) TEM micrograph of nano-particles and (b and c) SEM micrographs of micro-particles.

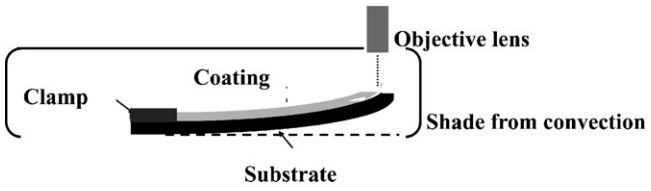

Fig. 2. Schematic illustration of the operation device for stress measurement.

2.2. Rheological measurements

A cone-plate viscometer (VIII-Rhometer, BROOKFIELD, Middleboro, Massachusetts, USA) was used for the rheological measurement taken in a shear rate range of 5–80 s^{-1}. The apparent viscosity was measured as a function of water content for the nano-slurries with pH 1.5, and as a function of pH value for the nano-slurries with 75 wt% water content. Moreover, the apparent viscosity of the 'binary particle' slurries was also measured as a function of the micro-particle size.

2.3. Stress measurement

The stress, generated during drying, was measured in situ using a substrate reflection method.[9,15] Schematic illustration of the operation device is shown in Fig. 2. A Fecralloy film (50 μm thick, Fe72.8/Cr22/Al5/Y0.1/Zr0.1, Goodfellow, Cambridgeshire, UK) was used as a substrate and was ground on both sides using SiO_2 paper (P600). After grinding, no apparent thickness variation was measured for the substrate, which was cut into rectangular pieces of 4 mm × 24 mm, and was cleaned in an ultrasonic bath. Slurry was cast on the substrate in a rectangular shape, 4 mm × 20 mm, with as-cast thickness around 300 μm. Thereafter, the coated substrate was immediately clamped at one end (4 mm × 4 mm) on a glass plate and put beneath the objective lens of a calibrated optical microscope (200×, Olympus BH, Tokyo, Japan). Displacement of the free end of the substrate was recorded every one minute by adjusting the focus. Simultaneously, images of the coating surface were taken in situ using a video camera (Zeiss, Dresden, Germany). During experiments, the coating was shielded to reduce the effect of convection. The average in-plane stress, $\sigma(t)$, could be calculated using the measured displacement of the substrate end, d[16]:

$$\sigma(t) = \frac{dE_s {h_s}^3}{3h_c(t)L^2(h_s + h_c(t))(1-\nu_s)} + \frac{dE_c(t)(h_s + h_c(t))}{L^2(1-\nu_c(t))} \quad (1)$$

where E_s, ν_s, h_s and L are, respectively, the elastic modulus, Poisson's ratio, thickness and un-clamped length of the substrate, $E_c(t)$, $\nu_c(t)$ and $h_c(t)$ are, respectively, the elastic modulus, Poisson's ratio and thickness of the coating which vary with time. In the derivation of Eq. (1), Corcoran[16] showed that the second term could be ignored without inducing large errors as long as $E_s \gg E_c(t)$ and/or $h_s \gg h_c$, as in most particulate coatings on rigid substrates.[13,14] It is reasonable to believe that the Young's modulus of a wet coating is extremely low in comparison to the Fecralloy substrate. In this study, the thicknesses of dried coatings are in a range of 40–140 μm, which are close to or higher than the substrate thickness. The omission of the second term will underestimate the real stress in the coating. However, Kinnemann et al.[9] experimentally proved that neglecting the second term of Eq. (1) did not apparently affect the stress plot when the coating thickness was in the same range of the substrate thickness. Therefore, only the first term in Eq. (1) was used for stress analysis here. The substrate properties are used as following: $E_s = 200$ GPa (measured using nano-indentation (Nano Instruments, MTS systems corporation, USA)), $\nu_s = 0.25$ (from the data provided by the supply company), $h_s = 50$ μm and $L = 20$ mm. Because lateral drying induced non-uniform thickness across the coating surface[11,12] which could not be monitored in this study, average in situ coating thickness was determined as

$$h_c(t) = h_i - \frac{h_i - h_f}{t_t} t \quad (2)$$

where h_i, h_f are, respectively, the initial coating thickness (300 μm) and the final coating thickness measured using the calibrated optical microscope, and t_t is the time required for the coating thickness reduction.

When the stress was measured, a coating cast on the same substrate was measured to obtain in situ weight loss using a weight balance (Ohaus AB-S, Mettler-Toledo Ltd., Leicester, UK) with a sensitivity of 0.01 mg.

All drying experiments were carried out in an ambient environment. A digital hydrothermal meter was used to record the drying conditions, with temperature of 22–22.5 °C and relative humidity of 55–60%. For each experiment, at least three samples were repeated, and the results were reproducible.

3. Results

3.1. Rheological behaviour

Figs. 3 and 4, respectively, compare viscosity versus shear rate for the nano-slurries with different water contents and pH values. As expected, decreasing the water content increases the viscosity. At low water content, particles occupy a large volume of the slurry, the attractive van der Waals force is significant

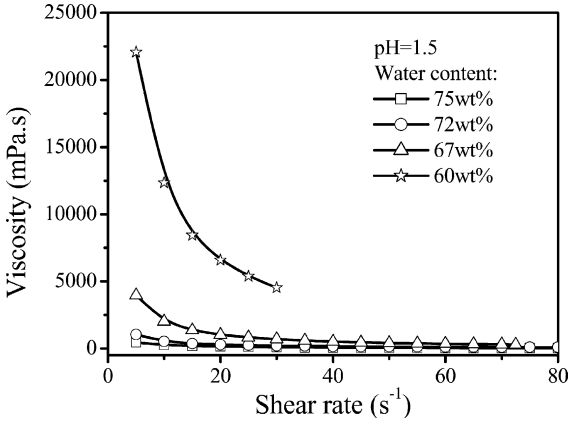

Fig. 3. Viscosity versus shear rate for the nano-slurries with pH 1.5 but different water contents.

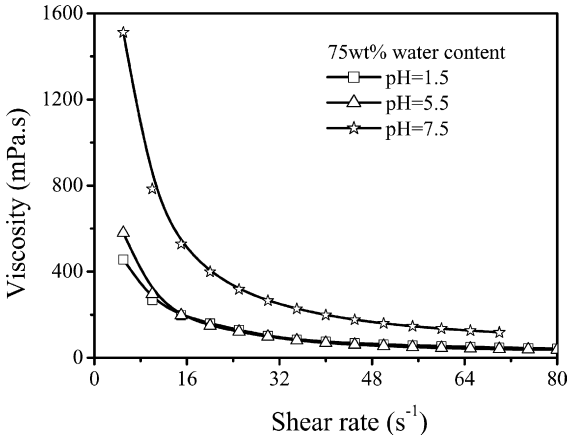

Fig. 4. Viscosity vs. shear rate for the nano-slurries with 75 wt% water content but with different pH values.

and the electrical double layer is compressed, resulting in high viscosity (Fig. 3). Holding the water content constant at 75 wt% (Fig. 4), the nano-slurry with pH 7.5 shows high viscosity and strong shear thinning behaviour, indicating high agglomeration degree.[17] This is attributed to the comparatively lower zeta potential at a pH value close to the IEP of YSZ particles which has been determined as around 8.[12] The repulsive forces between particles are too small to overcome the attractive van der Walls forces, resulting in the formation of a flocculated network. With decreasing pH away from the IEP, the repulsive forces increase. The slurry with pH 1.5 shows the lowest viscosity, suggesting that the particles are repulsive and well dispersed. The slurry with pH 5.5 shows a medium viscosity, in which particles are weakly attractive.

Micro-particles were added to the nano-slurry with pH 1.5 and 75 wt% water content to prepare 'binary particle' slurries. With the volume ratio 1:5 between nano-particles and micro-particles, the water content became 33 wt%. Because the viscosity of the nano-slurry with 33 wt% water content is too high to be measured, the viscosity of the nano-slurry with 75 wt% water content is compared with those of 'binary particle' slurries in Fig. 5. Though the water content of the nano-slurry (75 wt%) is much higher than that of the 'binary particle' slurries

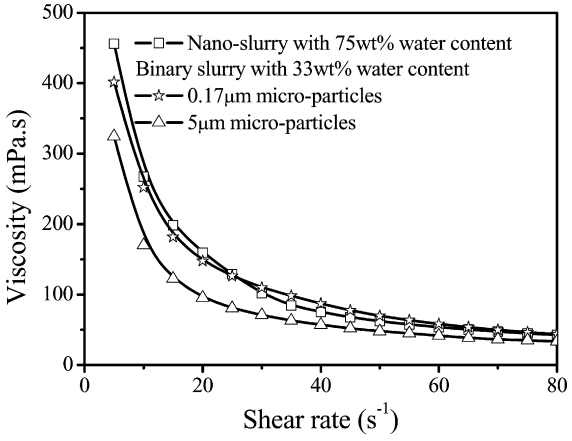

Fig. 5. Viscosity vs. shear rate for the nano-slurry and 'binary particle' slurries.

(33 wt%), the nano-slurry shows both high viscosity and strong shear thinning behaviour, indicating the particle size also plays a role in determining the slurry viscosity. In the mixing process, the nano-particles prefer to collide with micro-particles,[18] which can be further driven by repulsive interactions between the nano-particles which are highly positively charged ($\xi = 35.5$ mV) plus a weak attraction between the neutral micro-particles and the nano-particles.[19] As a result, the nano-particles form a coating layer on the surface of micro-particles and the average particle size increases, resulting in low viscosity.[20] Because the viscosity is inversely proportional to particle size at the same water content, the 'binary particle' slurry containing 5 μm micro-particles shows lower viscosity than that containing 0.17 μm micro-particles.

3.2. Stress development of coatings from nano-slurry

Fig. 6 shows the stress evolution, drying rate (V_{drying}) and drying rate differentiation against drying time (dV_{drying}/dt) as a function of residual water content for a well-dispersed nano-slurry with pH 1.5 and 50 wt% initial water content, coupled with optical images of the coating surface which correspond to specific stresses labeled by numbers. The residual water content (referred to as RWC later) is defined as the water weight in a wet coating over the in situ weight of the wet coating. In general, the drying rate decreased in the drying process, as shown in Fig. 6b. At the start of drying (RWC > 30 wt%), the drying rate decreased slightly, showing nearly constant dV_{drying}/dt (Fig. 6c), which was followed first by a gradual drying rate decrease in the RWC range from 30 to 15 wt% and then a steep decrease in the RWC range from 15 to 9 wt%. Thereafter, the rate of change of the drying rate decreased. When RWC > 30 wt%, the coating surface became dark and two domains, consisting of an outer dark region and an inner grey region, were visible and marked using a black line (Fig. 6 image 3). Meanwhile, no significant stress was measured and the coating stayed in a stress free state (Fig. 6a). A previous study[11] has proved that the color of the coating surface was related to the water content, i.e. the lower the water content, the darker the coating surface was. So the appearance of two domains suggested a lateral drying process. Solid particles were densely packed at the coating edge (dark region), while the excess of water remained at the coating centre (grey region). With continuous evaporation, the inner grey region became darker and shrank in size, whereas, the outer region became transparent and extended toward the centre (Fig. 6 image 4). The transparency allowed the rough substrate to be seen through the top coating as a result of the small spaces between nano-particles which are smaller than the wavelength of visible light. Interestingly, when the transparent region appeared at the coating edge, the drying rate deviated from a constant value and the stress rose in the coating. Cracks were first formed at the coating edge (Fig. 6: images 6 and 7), which accompanied further increase of the stress. The peak stress was reached at RWC = 15 wt% when the whole coating became transparent (Fig. 6: image 7). Subsequently, the stress decreased quickly to zero, accompanied by cracking of the coating into fragments and delamination from the substrate.

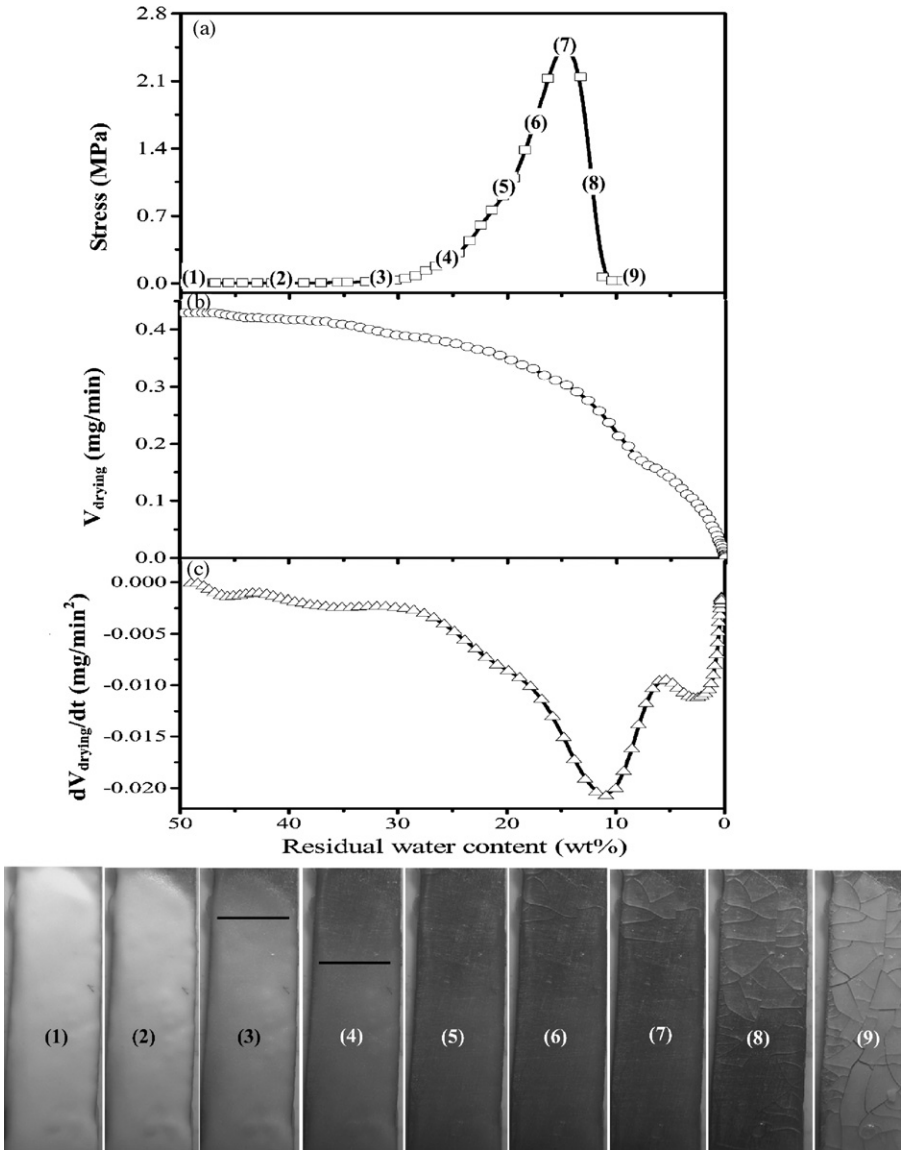

Fig. 6. Stress evolution, drying rate (V_{drying}) and drying rate differentiation against drying time (dV_{drying}/dt) for the nano-slurry with pH 1.5 and 50 wt% initial water content. Optical images correspond to specific stress evolution labeled by numbers.

3.3. Effect of initial water content

Fig. 7 compares the stress evolutions, drying rates and drying rate differentiations for the nano-slurries with pH 1.5 but different initial water contents, coupled with the optical images of the coating prepared from the dilute slurry with 70 wt% initial water content. Irrespective of the initial water content, both the stress evolution plots (Fig. 7a) and the drying rate plots (Fig. 7b) follow a similar shape for the three slurries. The stress history exhibits an initial stress-free state and then a rapid period of stress increase followed by a maximum stress and a subsequent stress decay to zero, which is typical for particulate coatings.[6–10] Interestingly, the stress increase appears to coincide with the time when the drying rate deviates from a constant value, as indicated by arrows, and the edge region becomes transparent. With increase in the initial water content, both the stress and the transparent region appear at higher RWC. Because cracks form at an early stage of drying and propagate when the central fluid region shrinks in size, the stress increase is more gradual for the coating from the nano-slurry with 70 wt% initial water content (Fig. 7a). When the same RWC is left in the coating, lower drying rate is obtained for the nano-slurry with higher initial water content due to smaller supersaturated region.[11]

3.4. Effect of pH value

Fig. 8 compares the stress evolutions, drying rates and drying rate differentiations for the nano-slurries with 50 wt% initial water content but different pH values, coupled with the optical images of the coating prepared from the agglomerated slurry with pH 7.5. With increases in pH value, i.e. increase in agglomeration degree, the stress rises earlier at higher RWC (Fig. 8a enlarged plots), but the drying rate deviates from a constant value

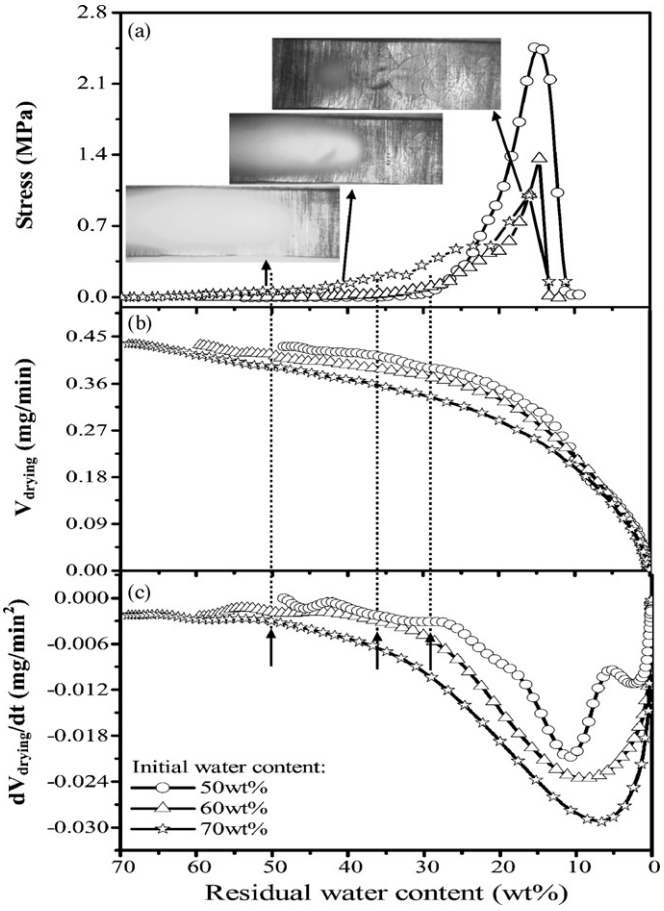

Fig. 7. Stress evolution, drying rate (V_{drying}) and drying rate differentiation against drying time (dV_{drying}/dt) for the nano-slurries with pH 1.5 but different initial water contents. Optical images are for the slurry with 70 wt% initial water content.

at lower RWC (Fig. 8c). In contrast with the well dispersed slurry with pH 1.5 of which the stress increase coincides with the drying rate deviation (Fig. 7), no apparent relation between stress increase and drying rate deviation is observed for the agglomerated slurries. Moreover, less apparent lateral drying and earlier cracking are observed in the coating from agglomerated slurries which shows uniform color across the coating surface (Fig. 8 images), and has been explained in detail in a previous paper.[12]

3.5. Effect of the addition of micro-particles

Drying of the nano-slurries led to cracking and delamination of coatings, regardless of the slurry composition. Micro-sized particles were added to the well-dispersed nano-slurry with pH 1.5. Due to strong particle attractions, the nano-slurry with 26 wt% water content is too viscous to form uniform coatings. The stress evolution of the nano-slurry with 50 wt% initial water content is compared with those of the 'binary particle' slurries with 26 wt% initial water content in Fig. 9, coupled with the optical images of dried coatings. With the addition of micro-particles, crack-free coatings were produced with good adhesion to substrates. The adhesion between the coating and the substrate could be judged by shaking the coating without peeling-off phenomenon. Compared with the drying of nano-slurries, the stress history of the 'binary particle' slurries shows the following features: (1) stress arises at lower residual water content, (2) lower peak stress is reached and (3) non-zero residual stress remains in the coating.

4. Discussion

4.1. Lateral drying

Observation using optical microscopy suggested lateral drying for the coatings prepared from nano-slurries (Figs. 6 and 7: images). When the water content was high, free particles were contained in the lateral flow which was driven by the capillary force from the central fluid region toward the outer densely-packed region at the coating edge.[11,12] At the central region, increase in particle concentration due to water evaporation was offset by decrease in particle content due to losing particles to the coating edge. Therefore, the central region of the coating with higher initial water content remained fluid until latter drying (Fig. 7: images). With decrease in the water content or increase in the agglomeration degree, the movement of particles was restricted by neighboring particles due to the increased attractive van der Waals force. Thus, fewer free particles could be transported in lateral flow and the lateral drying phenomenon became less significant (Figs. 6–8: images).

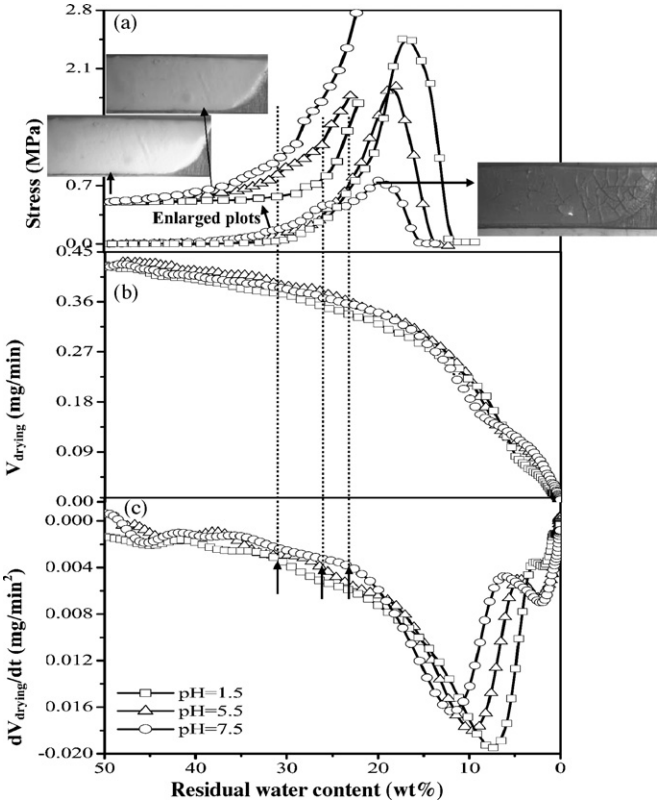

Fig. 8. Stress evolution, drying rate V_{drying} and drying rate differentiation against drying time (dV_{drying}/dt) for the nano-slurries with 50 wt% initial water content but different pH values. Optical images are for the slurry with pH 7.5.

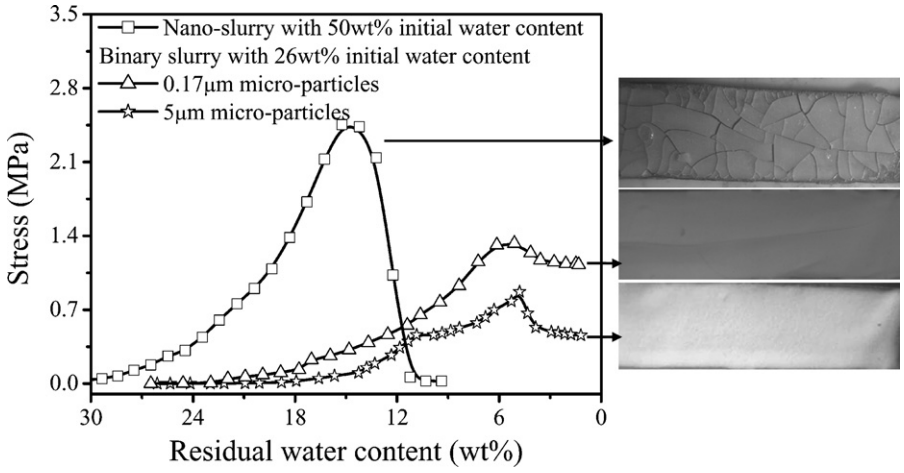

Fig. 9. Stress evolution as a function of residual water content for the nano-slurry and 'binary particle' slurries. Coupled with optical images of dried coatings.

The capillary length, l, over which the lateral flow can be transported, is given by[8]

$$l = \left[\frac{2hP_{\text{cap}}(1-\phi)^3}{5\dot{V}_{\text{E}}\eta_{\text{L}}(S\phi\rho_{\text{S}})^2}\right]^{1/2} \quad (3)$$

$$\phi = \frac{1-\text{RWC}}{1+5.05\text{RWC}} \quad (4)$$

$$P_{\text{cap}} = -\frac{2\gamma_{\text{LV}}\cos\theta}{r_{\text{pore}}} \quad (5)$$

$$r_{\text{pore}} \approx r_{\text{h}} = \frac{2(1-\phi)}{\phi\rho_{\text{S}}S} \quad (6)$$

where h is the thickness of coating, $\dot{V}_{\text{E}}$ the evaporation rate, P_{CRP} the capillary pressure at 100% saturation, η_{L} the viscosity of water, ϕ, S, and ρ_{S}, respectively, the volume fraction, specific surface area and theoretical density of solid particles, γ_{LV} the surface tension of water (72 dyn/cm), r_{pore} the pore radius and can be approximated using hydraulic radius and r_{h},[21] and θ is the water contact angle on YSZ particles (25°[22]).

Theoretical density of YSZ particles $\rho_{\text{S}} = 6.05 \times 10^3$ kg/m^3; the viscosity of water $\eta_{\text{L}} = 1.3$ mPa s from a literature[23]; $V_{\text{E}} = 8.9 \times 10^{-8}$ m/s, is calculated using the average drying rate, 0.43 mg/min, in the early drying stage (Fig. 6b); S is measured using a BET method; h is approximated by the average dried coating thickness measured using calibrated optical microscope; ϕ is approximated by the solid volume fraction of circular coatings at the CRP end point which can be calculated using RWC according to Eq. (5); P_{cap} is calculated using Eq. (6). Table 1 lists the experimental parameters and calculated capillary length. For the tested slurries, the capillary length is shorter than the coating half-length, 10 mm. That means when the coating edge reaches saturation, not enough water can be sucked from the central fluid region to keep the edge saturated. The air–water interface recedes into pores, which induces the decrease in the drying rate due to decreased evaporation area[11,12] and exerts a big compressive force in the solid structure.[5] Because the coating is adhered to the substrate, tensile stress arises in the coating. This is consistent with the experimental results, which show that the appearance of a transparent region at the coating edge coincides with the stress increase and the drying rate deviation from a constant value (Figs. 6 and 7). Transparency represents water saturation in this study. It is also noted that increase in initial water content decreases the capillary length (Table 1), leading to earlier saturation at the coating edge (Fig. 7: images), while, increase in the pH value increases the capillary length, resulting in less apparent lateral drying and more constant drying rate (Fig. 8).

4.2. Stress evolution

As a coating is densified by drying, it shrinks in the thickness direction because the in-plane contraction is resisted by the substrate. In early drying, the cast slurry is fluid enough that any constrained stress is immediately relieved by viscous flow. Therefore the coating stays in a stress free state (Figs. 6–8). As drying proceeds, the particles move to each other to form a rigid

Table 1
Calculated capillary length for the tested nano-slurries

pH	Initial water content (wt%)	S ($\times 10^4$ m^2/kg)	Dried coating thickness (μm)	RWC at CRP end point (wt%)	P_{CRP} ($\times 10^7$ Pa)	Capillary length (mm)
1.5	70	7.8	40	25	1.53	5.1
1.5	60	7.8	72	22	1.81	6.1
1.5	50	7.8	114	19	2.17	6.6
7.5	50	7.4	138	21	1.91	7.9

S: specific surface area measured using BET method; RWC: residual water content; CRP: constant rate period; P_{CRP}: capillary force at the CRP end point.

structure under attractive van der Waals forces which can support a tensile stress resulted from the constrained volume shrinkage. Thus, the appearance of tensile stress represents the transition of the slurry from viscous to viscoelastic which is determined by the slurry viscosity. The slurry viscosity is controlled by the solid fraction (Fig. 3) and the interparticle potentials (Fig. 4). Rigid structures form at higher water content in agglomerated slurries because of the lower repulsive electrostatic force. This is consistent with experimental results which show the higher the agglomeration degree, the earlier the stress rises (Fig. 8). Lateral drying leads to non-uniform water distribution across the coating surface. Due to shorter capillary length, saturation is reached sooner at the edge of the coating from the dilute nano-slurry, resulting in an earlier stress increase at higher RWC (Fig. 7).

During drying, cracks are formed first at the coating edge (Figs. 6–8: images), which release the tensile stress. The competition between stress release by cracking and stress increase due to increased rigid region, i.e. transparent region in this study, brings a further stress increase, as shown in Figs. 6–8. The peak stress is reached when the whole coating becomes saturated, i.e. the central grey region disappears and the whole coating becomes transparent, which is consistent with the origin of the tensile stress from capillary forces which reaches the maximum at 100% saturation. However, the measured peak stresses in Figs. 6–8 are much lower than the calculated capillary forces in Table 1. The difference results from cracking and coating delamination which release part of the tensile stress. The measured peak stress is only from the crack-free area. Taking the drying of the slurry with pH 1.5 and 50 wt% initial water content as an example, the crack-free length is 14.4 mm (Fig. 6: image 7) which is close to the double value of the calculated capillary length of 13.2 mm (Table 1), further proving that the coating in the range of capillary length can be saturated with water. The peak stress in Fig. 6 is corrected to be 6.6 MPa by setting L as 14.4 mm in Eq. (1), which is reasonably consistent with the calculated capillary force, 18 MPa, taking into account the underestimation caused by the omission of the second term in Eq. (1).

With addition of micro-particles to the nano-slurry, the viscosity decreases significantly (Fig. 5). Therefore, particles form a rigid structure at much lower residual water content in the 'binary particle' slurries in comparison with the nano-slurry, resulting in the later appearance of the tensile stress (Fig. 9). Because pore size is related to particle size, the addition of micro-particles leads to an increase in average pore size within the coating. According to Eq. (5), the capillary force is inversely proportional to the pore size. Lower capillary force develops in the coating from 'binary particles' slurries, resulting in lower tensile stress (Fig. 9) which is not big enough to crack the coatings. Therefore, integrating coatings are prepared from the 'binary particle' slurries.

5. Conclusions

The relation between lateral drying and stress evolution has been investigated using the coatings prepared from aqueous YSZ slurries. Tensile stress built up when the coating edge reached saturation with water and the drying rate deviated from a constant value. Peak stress was obtained when the central fluid region disappeared and was proportional to the crack-free area. The addition of micro-particles to the nano-slurry resulted in a later stress increase due to the decreased viscosity of the slurry and lower peak stress due to larger average particle size.

Acknowledgement

Mel Chemicals is acknowledged for providing YSZ slurry.

References

1. Lewis, J. A., Blackman, K. A., Ogden, A. L., Payne, J. A. and Francies, L. F., Rheological properties and stress development during drying of tape-cast ceramic layers. *J. Am. Ceram. Soc.*, 1996, **79**(12), 3225–3234.
2. Lange, F. F., Chemical solution routes to single-crystal thin films. *Science*, 1996, **273**, 903–909.
3. Wang, X., Lan, W. H. and Xiao, P., Fabrication of yttria stabilised zirconia coatings by a novel slurry method. *Thin Solid Films*, 2006, **494**(1–2), 263–267.
4. Wang, Z. C., Shemilt, J. and Xiao, P., Fabrication of ceramic composite coatings using electrophoretic deposition, reaction bonding and low temperature sintering. *J. Eur. Ceram. Soc.*, 2002, **22**(2), 183–189.
5. Scherer, G. W., Theory of drying. *J. Am. Ceram. Soc.*, 1990, **73**(1), 3–14.
6. Chiu, R. C., Garino, T. J. and Cima, M. J., Drying of granular ceramic films. I. effect of processing variables on cracking behaviour. *J. Am. Ceram. Soc.*, 1993, **76**(9), 2257–2264.
7. Chiu, R. C. and Cima, M. J., Drying of granular ceramic films. II. Drying stress and saturation uniformity. *J. Am. Ceram. Soc.*, 1993, **76**(11), 2769–2777.
8. Guo, J. J. and Lewis, J. A., Aggregation effects on the compressive flow properties and drying behavior of colloidal silica suspension. *J. Am. Ceram. Soc.*, 1999, **83**(9), 2345–2358.
9. Kinnemann, J., Chartier, T., Pagnoux, C., Baumard, J. F., Huger, M. and Lamerant, J. M., Drying mechanisms and stress development in aqueous alumina tape casting. *J. Eur. Ceram. Soc.*, 2005, **25**, 1551–1564.
10. Wedin, P., Lewis, J. A. and Bergstrom, L., Soluble organic additive effects on stress development during drying of calcium carbonate suspensions. *J. Colloid Interf. Sci.*, 2005, **290**, 134–144.
11. Lan, W. H. and Xiao, P., Constrained drying of aqueous yttria-stabilised-zirconia slurry on a substrate. I. Drying mechanism. *J. Am. Ceram. Soc.*, 2006, **89**(5), 1518–1522.
12. Lan, W. H., Wang, X. and Xiao, P., Agglomeration effect on drying of yttria-stabilised-zirconia slurry on a metal substrate. *J. Eur. Ceram. Soc.*, 2006, **26**(16), 3599–3606.
13. Martinez, C. J. and Lewis, J. A., Shape evolution and stress development during latex-silica film formation. *Langmuir*, 2002, **18**, 4689–4698.
14. Tirumkudulu, M. S. and Russel, W. B., Role of capillary stresses in film formation. *Langmuir*, 2004, **20**, 2947–2961.
15. Tirumkudulu, M. S. and Russel, W. B., Cracking in drying latex films. *Langmuir*, 2005, **21**, 4938–4948.
16. Corcoran, E. M., Determining stress in organic coatings using plate beam deflection. *J. Paint. Technol.*, 1969, **41**, 635–640.
17. Lgoh, G. K., Donthu, S. K. and Pallathadka, P. K., Cracking and orientation of solution-deposited rutile TiO_2 films. *Chem. Mater.*, 2004, **16**, 2857–2861.
18. Bruinsma, P. J., Wang, Y., Li, X. Sh., Liu, J., Smith, P. A. and Bunker, B. C., Rhelogical and solid–liquid separation properties of bimodal suspensions of colloidal gibbsite and boehmite. *J. Colloid Interf. Sci.*, 1997, **192**, 16–25.

19. Tohver, V., Chan, A., Sakurada, O. and Lewis, J. A., Nanoparticle engineering of complex fluid behavior. *Langmuir*, 2001, **17**, 8414–8421.
20. Lan, W. and Xiao, P., Constrained drying of aqueous yttria-stabilized-zirconia slurry on a substrate. II. Binary particle slurries. *J. Am. Ceram. Soc.*, submitted for publication.
21. Smith, D. M., Scherer, G. W. and Anderson, J. M., Shrinkage during drying of silica gel. *J. Non-Cryst. Solids*, 1995, **188**, 191–206.
22. Feng, A., McCoy, B. J., Munir, Z. A. and Cagliostro, D., Wettability of transition metal oxide surfaces. *Mater. Sci. Eng. A*, 1998, **242**, 50–56.
23. Salamanca, J. M., Ciampi, E. D., Faux, A., Glover, P. M., McDonald, P. J., Routh, A. F. *et al.*, Lateral drying in thick films of waterborne colloidal particles. *Langmuir*, 2001, **17**, 3202–3207.